Electronic Supplementary Information

Chelation-activated ultralong room-temperature phosphorescence and thermo-/excitation-dependent persistent luminescence

Siqin Wu, Bo Zhou, Xiaoyu Fang and Dongpeng Yan*

Beijing Key Laboratory of Energy Conversion and Storage Materials, College of Chemistry, and Key Laboratory of Radiopharmaceuticals, Ministry of Education, Beijing Normal University, Beijing 100875, P. R. China

Key Laboratory of Theoretical and Computational Photochemistry, Ministry of Education, College of Chemistry, Beijing Normal University, 100875 Beijing, P. R. China.

E-mail: yandp@bnu.edu.cn

Table of Contents

1. **Experimental Procedures**

2. **Figures (S1- S26) and Tables (S1- S5)**

3. **Supporting References**

1. Experimental Procedures

The large steric hindrance of 4HPDD makes it difficult to coordinate with metal ions directly, and thus we choose 4HPDA (4-Hydroxy-2,6-pyridinedicarboxylic acid) as the precursor. During the evaporation process, 4HPDA is esterified by CH_3OH into 4HPDD. The target structure cannot be obtained using 4HPDD as the precursor. We also introduced 1,10-phenanthroline (P) as the second ligand, to adjust the energy level of the material and to obtain tunable optical properties.

Materials and reagents. All the reagents (4-hydroxy-2,6-pyridinedicarboxylic acid, 1,10-phenanthroline, cadmium chloride, cadmium nitrate tetrahydrate, nitric acid and methanol) were purchased from Sigma Chemistry Co. Ltd. and used without further purification. Distilled water was prepared in the lab.

Synthesis of $CdCl_2$-4HPDD. 4-Hydroxy-2,6-pyridinedicarboxylic acid (0.1 mmol, 18.3 mg), cadmium chloride (0.1 mmol, 18.3 mg) and methanol (2 mL) were mixed into the 15 mL reaction vial. After keeping at 60 ℃ for 5 days, lamellar crystal can be obtained by evaporation of the solvent for another several days at ambient condition.

Synthesis of 4HPDD-$Cd(NO_3)_2$-P. 4-Hydroxy-2,6-pyridinedicarboxylic acid (0.1 mmol, 18.3 mg), phenanthroline (0.1 mmol, 18.0 mg), cadmium nitrate tetrahydrate (0.1 mmol, 30.8 mg), nitric acid (0.1 mL) and methanol (6 mL) were mixed into the 15 mL reaction vial. Yellowish-brown bulk crystal can be obtained by evaporation of the solvent for another several days at ambient condition.

Characterization. Single-crystal X-ray diffraction data of these samples were collected on an Oxford Diffraction SuperNova area-detector diffractometer using mirror optics monochromated Cu Kα radiation at 100 K. TGA tests were carried out on a Pekin-Elmer Diamond SII thermal analyzer from 25 to 500 ℃ under nitrogen atmosphere with a heating rate of 10 ℃/min. FTIR spectra was test on IRAffinity-1 Fouries Transform Infrared spectrometer. PXRD spectra was test on Rigaku Ultima-IV. UV-vis absorption spectra were performed on a Shmadzu UV-3600 spectrophotometer at room temperature. PL microscope images of crystals were taken under OLYMPUS IXTI fluorescence microscope. Nuclear magnetic resonance (^{1}H

NMR) spectra were obtained on a Bruker Ultra Shield Plus 600 MHz spectrometer. All the relevant PL tests and time-resolved lifetime were conducted on an Edinburgh FLS980 fluorescence spectrometer. The PLQY values were recorded by using a Teflon-lined integrating sphere (F-M101, Edinburgh) accessory in FLS980 fluorescence spectrometer.

Theoretical calculations. The calculations were performed with the density functional theory (DFT) and time-dependent density functional theory (TD-DFT) on the basis of Gaussian 09 software.[1] The initial configurations were fully optimized by ωB97XD[2] with lanl2dz basic set for Cd and 6-31+g(d) for the others. The natural transition orbitals (NTOs) were calculated through wavefunction analysis program Multiwfn.[3] The hole-electron distribution maps[4] were visualized through VMD software.[5] The spin-orbit coupling (SOC) matrix elements between singlet and triplet states was evaluated through ORCA package,[6, 7] (version 4.2.1) with ωb97x-d3 and def2-TZVP basic set in which relativistic effects were accounted for using the Zero Order Regular Approximation (ZORA).[8] Electronic structure and geometry optimization are based on the Vienna Ab Initio Simulation Package (VASP).[9] Meanwhile, the exchange-correlation interactions were represented by the Perdew-Burke-Ernzerhof (PBE) functional and the interactions between ionic cores and valence electrons were described by the projector-augmented wave (PAW) approach.[10] The plane-wave basis energy cutoff is set as 400 eV. A 1 × 1 × 1 Monkhorst−Pack *k*-point mesh is used in the geometry optimization and a 3 × 3 × 3 *k*-mesh is adopted for electronic structure.[11] The van der Waals interactions are described using the Grimme DFT-D3 method.[12]

2. Fig. S1-Fig. S25 and Table S1-Table S4

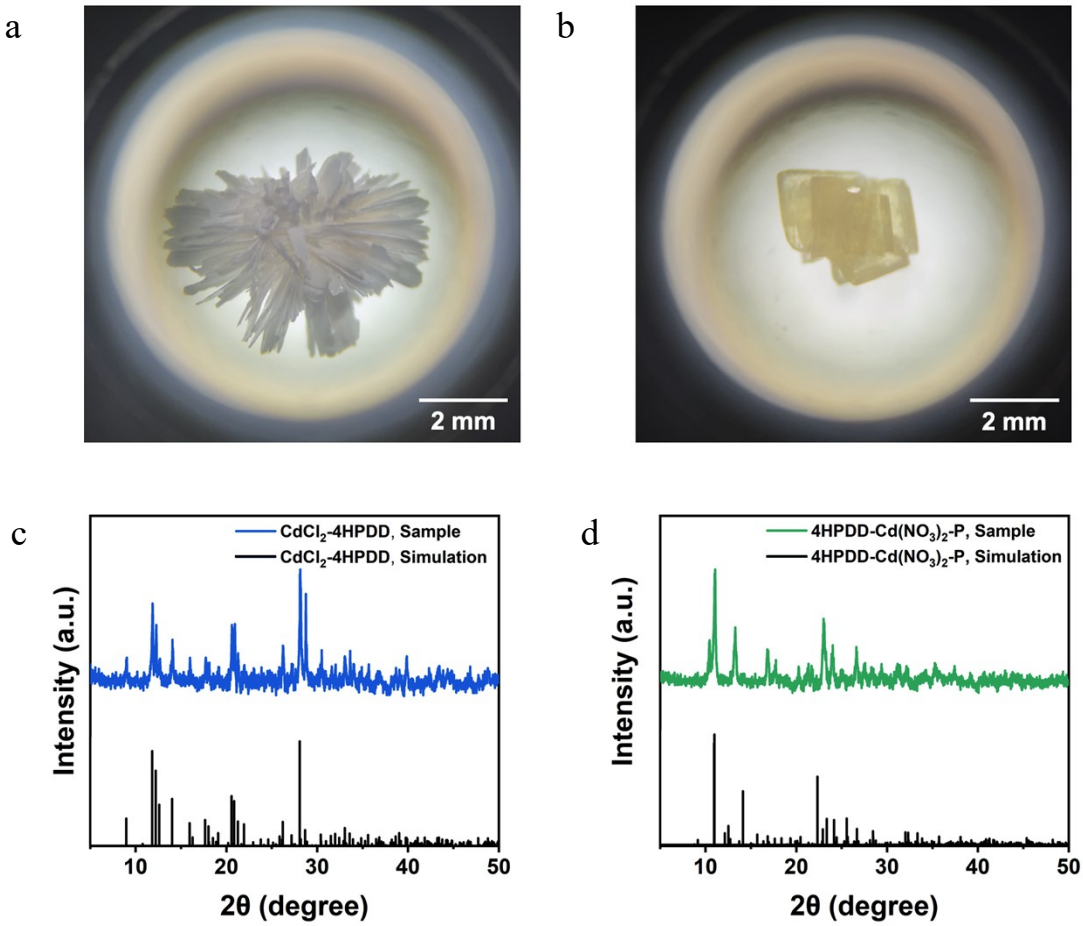

Fig. S1. The photos of $CdCl_2$-4HPDD (a) and 4HPDD-$Cd(NO_3)_2$-P (b) crystals. The as-synthesized and simulated PXRD patterns data of $CdCl_2$-4HPDD (c) and 4HPDD-$Cd(NO_3)_2$-P (d), respectively.

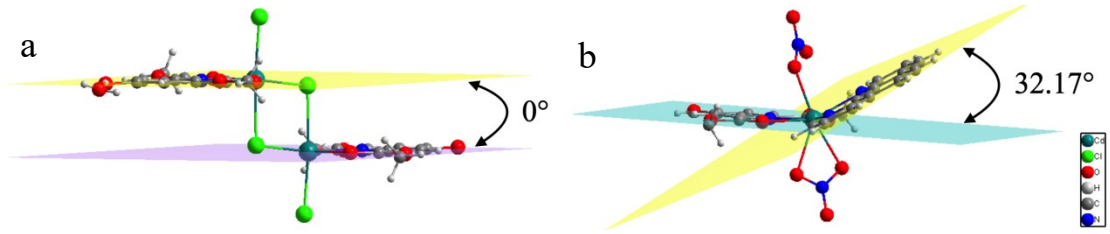

Fig. S2. The angle between two HPDD planes in $CdCl_2$-4HPDD (a) and the angle between HPDD and P planes in 4HPDD-$Cd(NO_3)_2$-P (b).

a

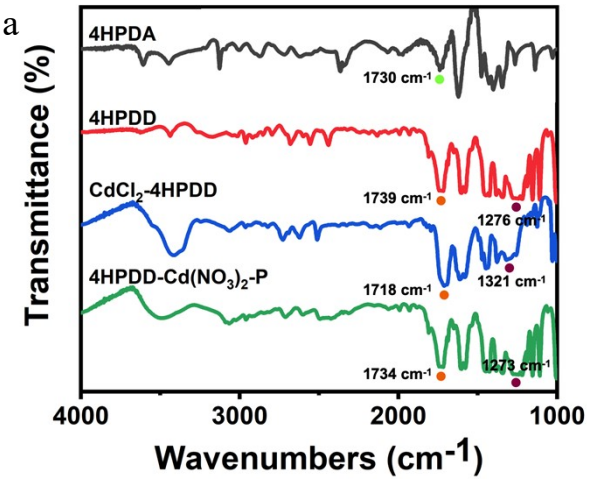
4HPDA
1730 cm-1
4HPDD
1739 cm-1
1276 cm-1
CdCl2-4HPDD
1718 cm-1
1321 cm-1
4HPDD-Cd(NO3)2-P
1734 cm-1
1273 cm-1
Transmittance (%)
4000
3000
2000
1000
Wavenumbers (cm-1)

b

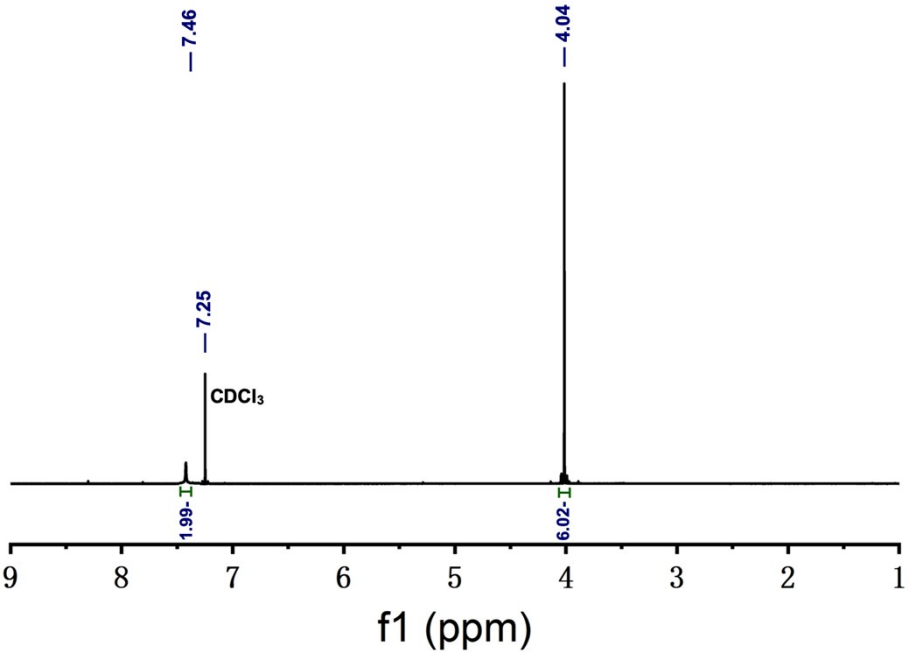
7.46
4.04
7.25
CDCl3
1.99
6.02
9
8
7
6
5
4
3
2
1
f1 (ppm)

c

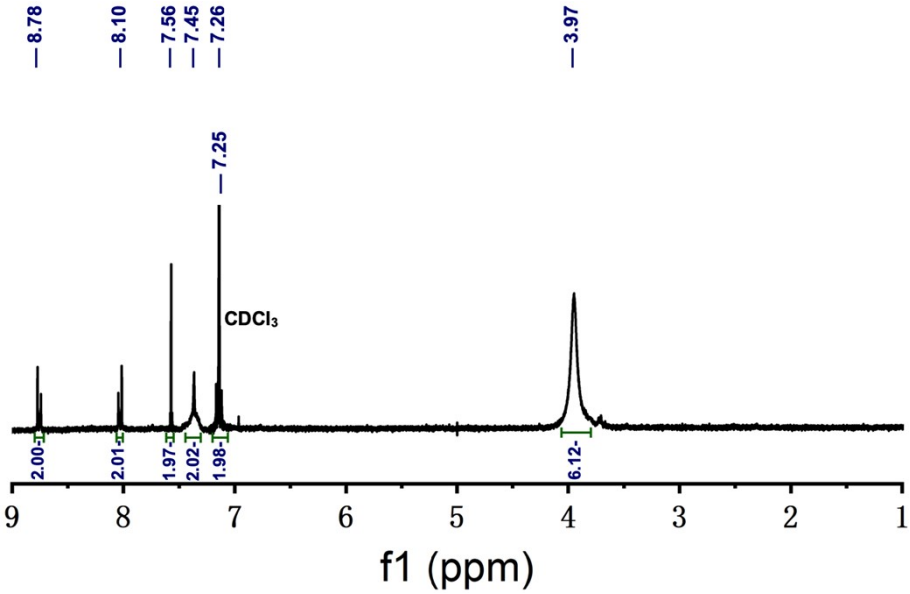
8.78
8.10
7.56
7.45
7.26
3.97
7.25
CDCl3
2.00
2.01
1.97
2.02
1.98
6.12
9
8
7
6
5
4
3
2
1
f1 (ppm)

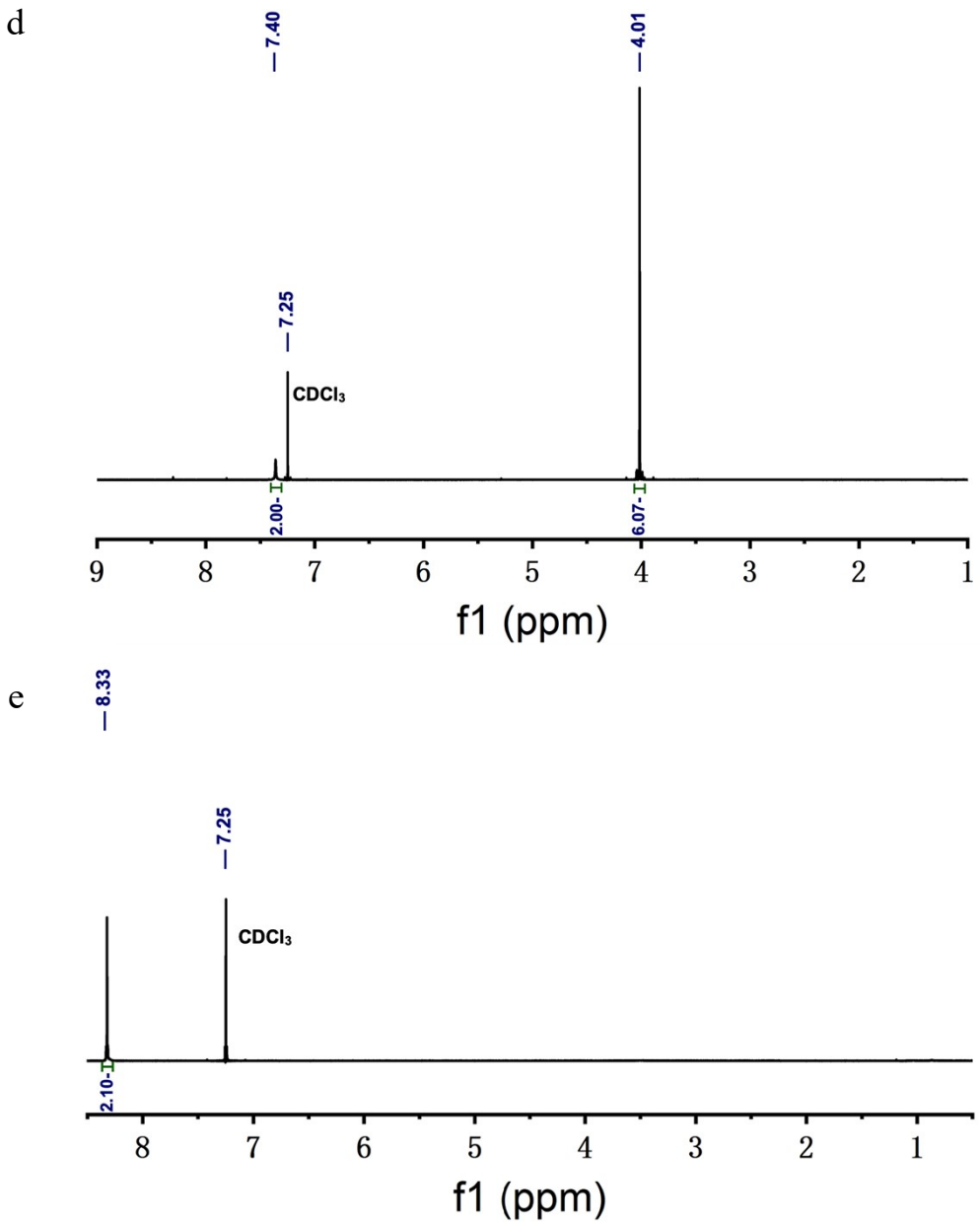

Fig. S3. Fourier transform infrared (FT-IR) spectra (a) of organic ligand 4HPDA, 4HPDD, and the as-prepared mononuclear $CdCl_2$-4HPDD and binuclear 4HPDD-$Cd(NO_3)_2$-P at room temperature. The ^1H NMR spectrum of $CdCl_2$-4HPDD (b), 4HPDD-$Cd(NO_3)_2$-P (c), 4HPDD (d) and 4HPDA (e) molecule in $CDCl_3$.

FT-IR spectra show that the absorption peaks from the ester carbonyl appear at 1739, 1718 and 1734 cm^{-1} in 4HPDD, $CdCl_2$-4HPDD and 4HPDD-$Cd(NO_3)_2$-P, respectively, demonstrating the esterification of 4HPDA. The weaker absorption peak at 1730 cm^{-1} in 4HPDA can be clarified as overtone of hydroxy stretch (O-H). Meanwhile, characteristic strong and broad bands of ester ($\nu^{as}_{C=O}$) can also be observed at 1276, 1321 and 1273 cm^{-1} for the 4HPDD, $CdCl_2$-4HPDD and 4HPDD-$Cd(NO_3)_2$-P, which

have not appeared in 4HPDA.

^{1}H NMR ($CDCl_3$): (b) $CdCl_2$-4HPDD: δ 4.04 (s, 6H), 7.46 (s, 2H). The peak of active hydroxyl hydrogen (-OH) does not appear in the spectrum; (c) 4HPDD-$Cd(NO_3)_2$-P: δ 3.97 (s, 6H), 7.26 (t, 2H), 7.45 (s, 2H), 7.56 (s, 2H), 8.10 (d, 2H), 8.78 (d, 2H). The peak of active hydroxyl hydrogen (-OH) does not appear in the spectrum; (d) 4HPDD: δ 4.01 (s, 6H), 7.40 (s, 2H). The peak of active hydroxyl hydrogen (-OH) does not appear in the spectrum; (e) 4HPDA: δ 8.33 (s, 2H). The peak of active hydroxyl hydrogen (-OH) and carboxyl hydrogen (-COOH) does not appear in the spectrum.

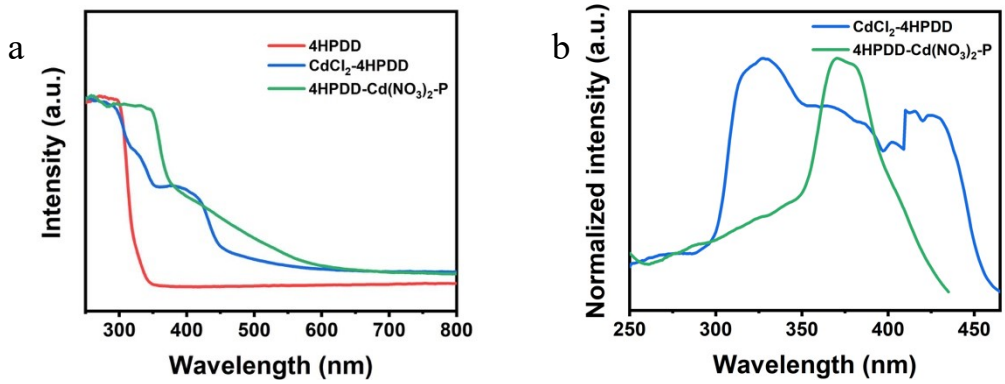

Fig. S4. (a) Solid-state UV-vis absorption spectra of organic ligand 4HPDD and the as-prepared mono/binuclear complexes under ambient conditions. (b) Excitation spectra of $CdCl_2$-4HPDD and 4HPDD-$Cd(NO_3)_2$-P.

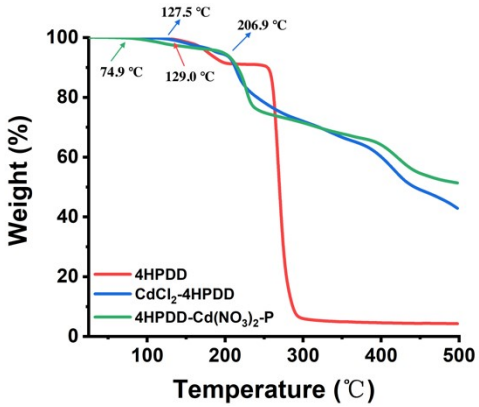

Fig. S5. The thermogravimetric analysis (TGA) curves of 4HPDD, $CdCl_2$-4HPDD and 4HPDD-$Cd(NO_3)_2$-P.

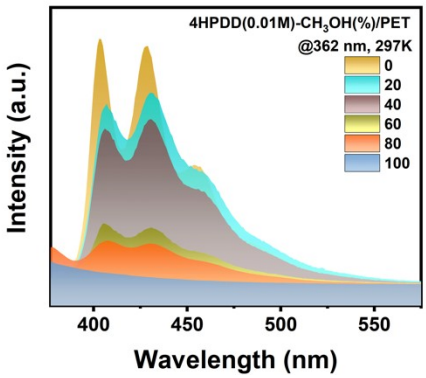

Fig. S6. Steady-state emission spectra (a) of 4HPDD in a bicomponent solution mixture showing the AIE process with different CH_3OH ratios (V_{CH3OH}/V_{total}, 4HPDD concentration: 1.0 x 10^{-2} mol/L).

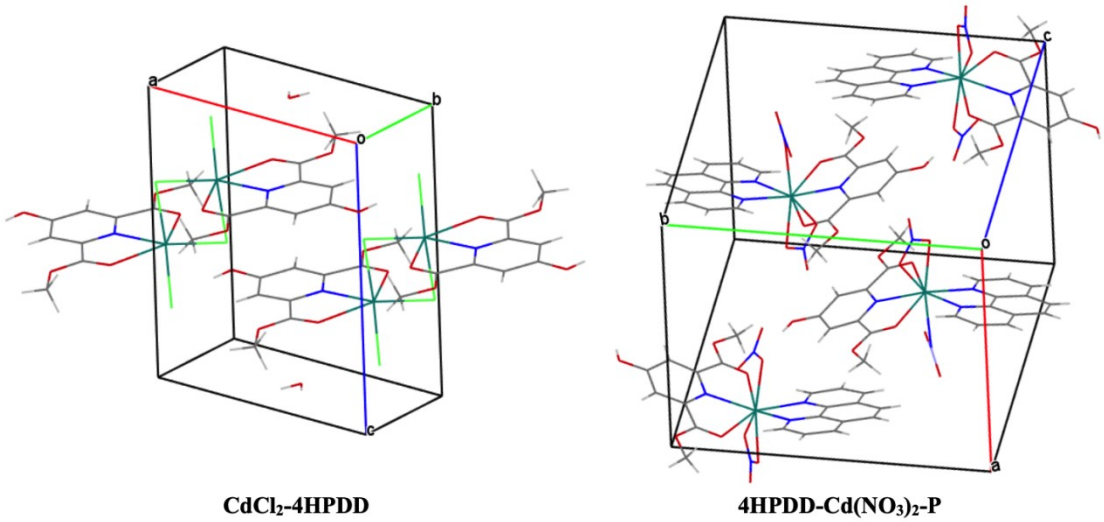

Fig. S7. The packing diagrams of $CdCl_2$-4HPDD and 4HPDD-$Cd(NO_3)_2$-P shown in wireframe model.

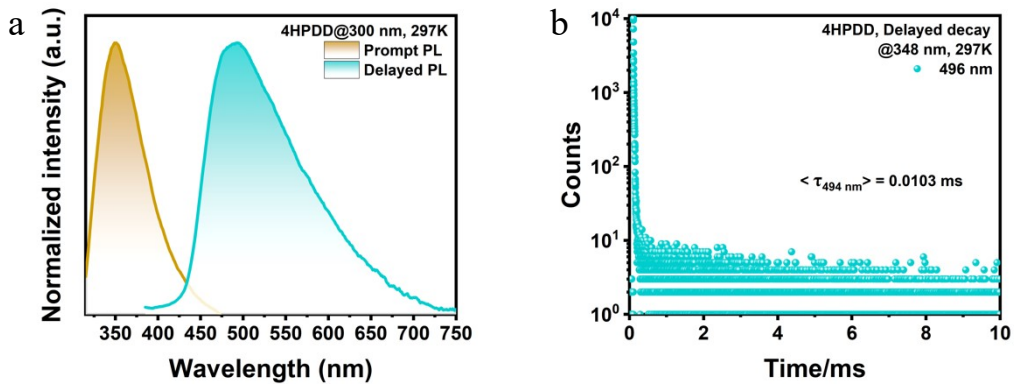

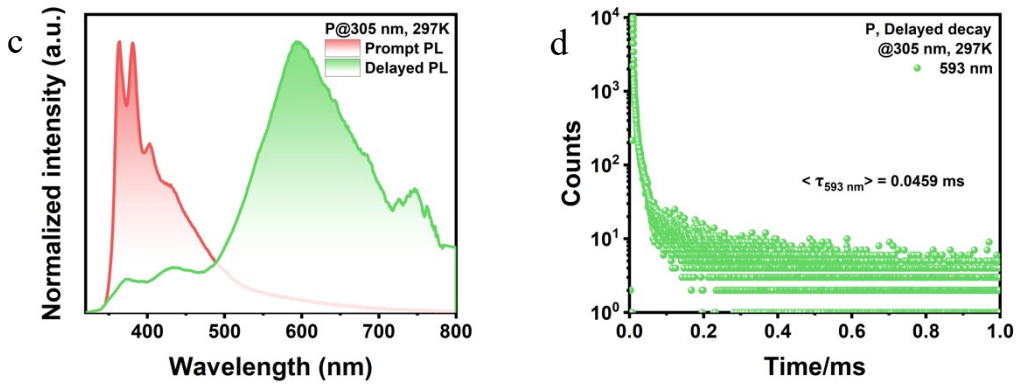

Fig. S8. The prompt and delayed PL spectra (**a and c**) and long-lived lifetime decay profiles (**b and d)** of 4HPDD and P at 297 K, respectively.

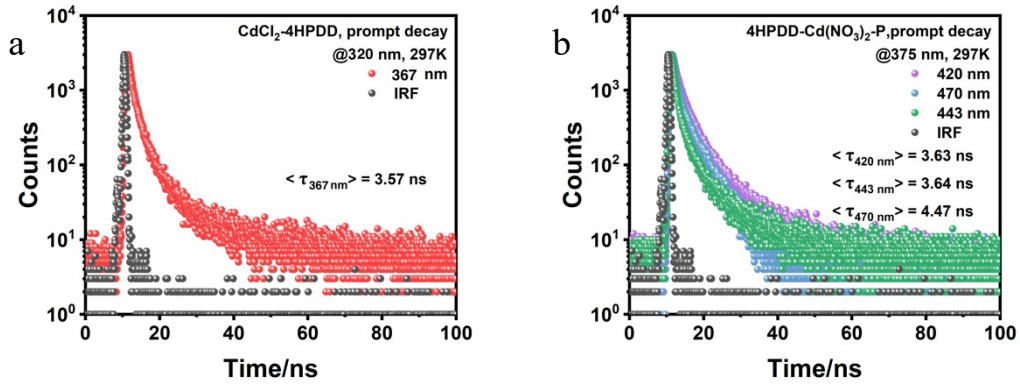

Fig. S9. The short-live lifetime profiles of $CdCl_2$-4HPDD (a) and 4HPDD-$Cd(NO_3)_2$-P (b) at 297K.

a

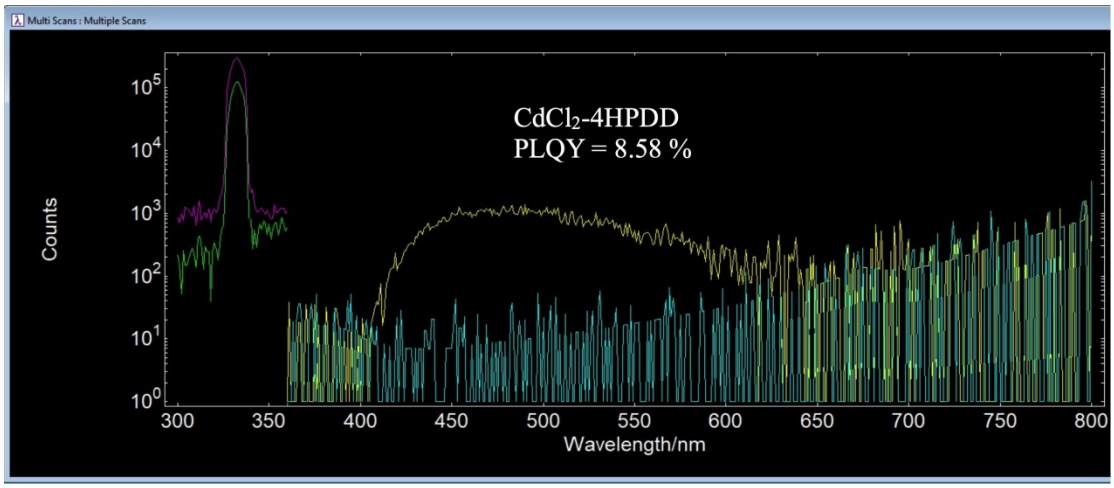

b

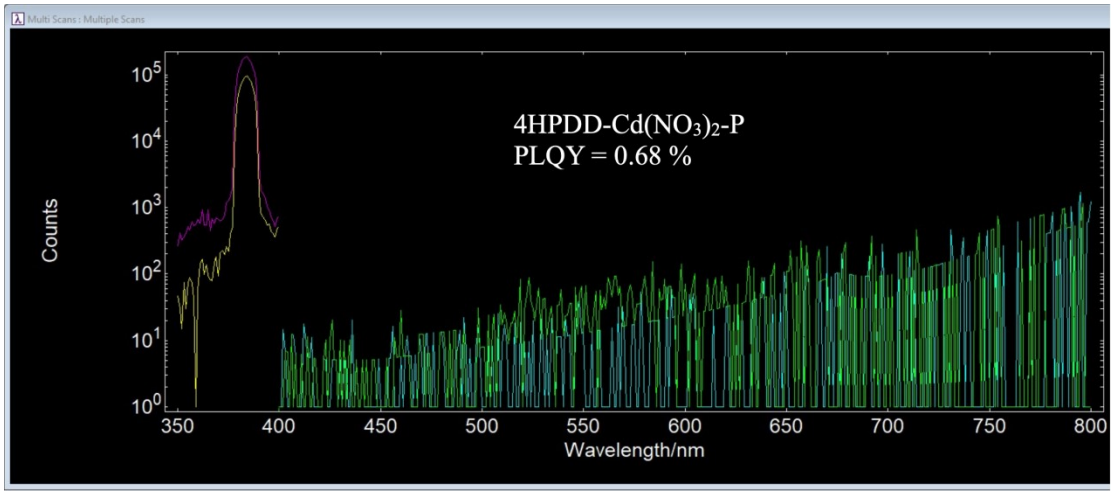

Fig. S10. The detailed measurement profiles of long-lived PLQY for $CdCl_2$-4HPDD (a) and 4HPDD-$Cd(NO_3)_2$-P (b) recorded in FLS980 fluorescence spectrometer.

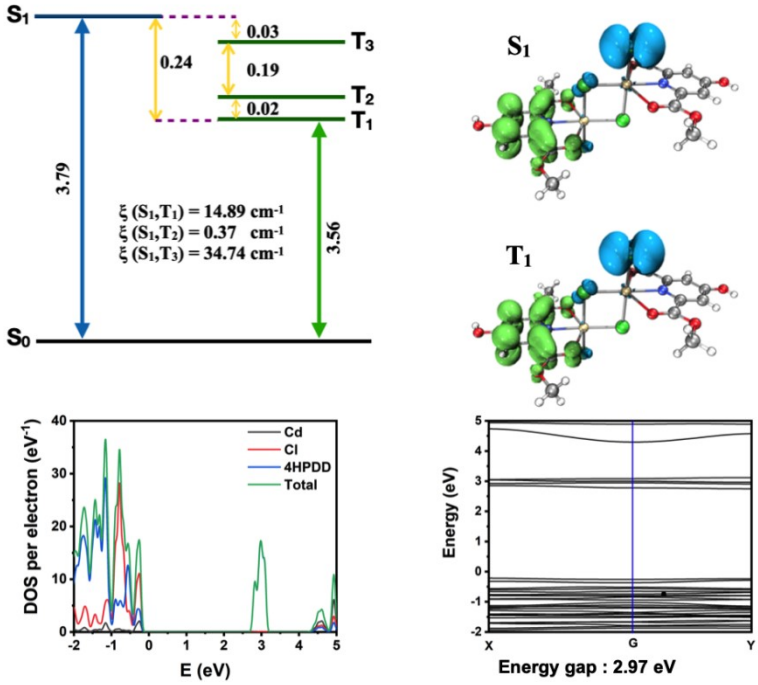

Fig. S11. Energy level diagrams and SOC constant, hole-electron analysis (holes and electrons are shown in blue and green, respectively) of the S_1 and T_1 based on the optimized geometries, band structures around Fermi energy level and the TDOS/PTDOS of states for $CdCl_2$-4HPDD.

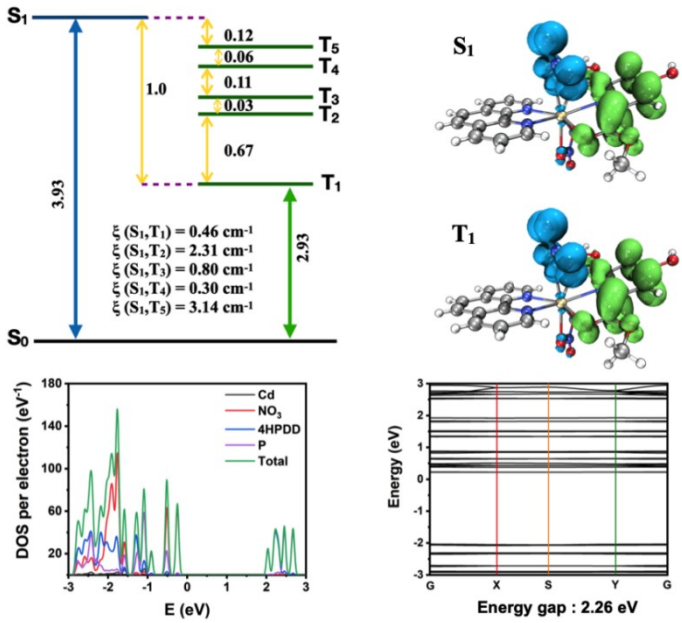

Fig. S12. Energy level diagrams and SOC constant, hole-electron analysis (holes and electrons are shown in blue and green, respectively) of the S_1 and T_1 based on the optimized geometries, band structures around Fermi energy level and the TDOS/PTDOS for 4HPDD-$Cd(NO_3)_2$-P (b).

The band structures, density of states (DOS) and electron-density distributions are obtained by using periodic DFT calculations (Fig. S11-15). The band structure calculation results indicate the theoretical energy gaps of $CdCl_2$-4HPDD and 4HPDD-$Cd(NO_3)_2$-P solids are 2.97 and 2.25 eV, respectively, which are corresponding to the experimental results calculated from the UV-vis absorption edge (2.57 and 2.20 eV), indicating that the delayed emissions are certainly originating from triplet states (Fig. S16).

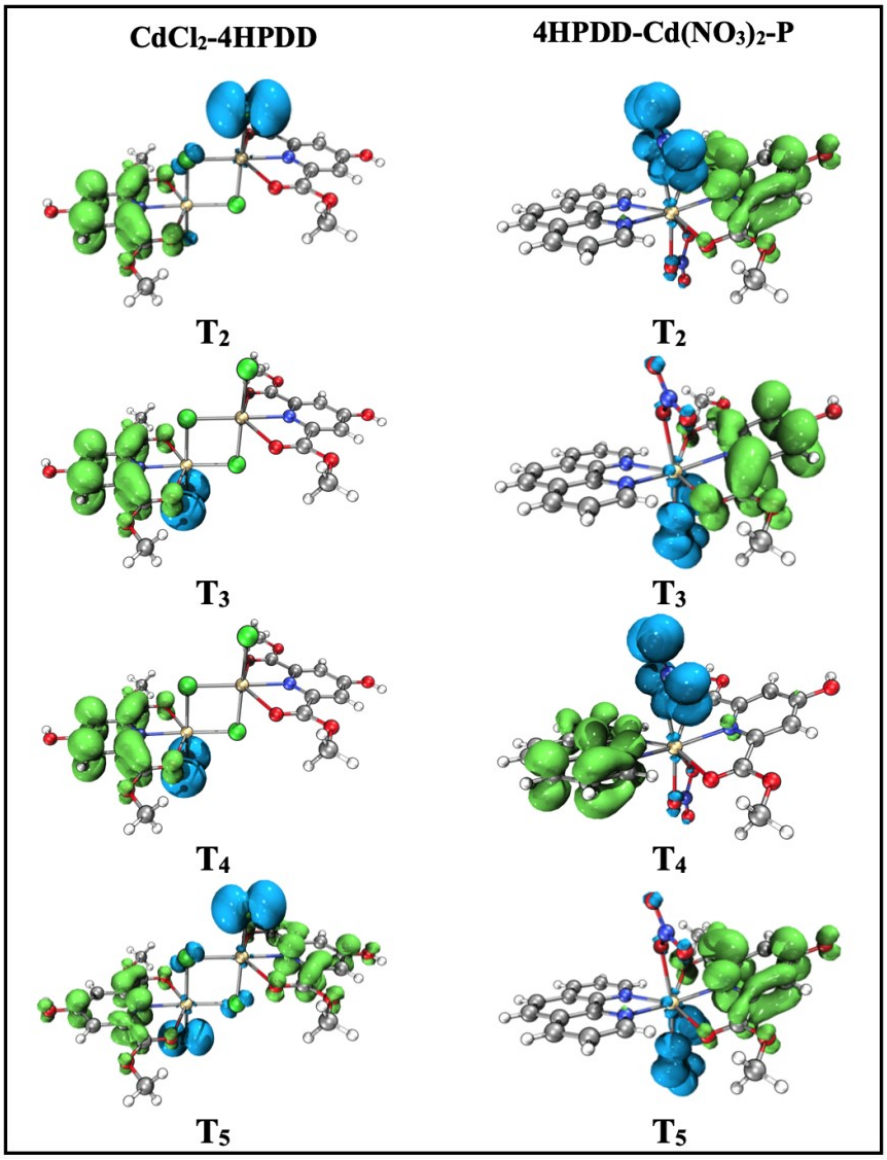

Fig. S13. Hole-electron analysis (holes and electrons are shown in blue and green, respectively) of T_n based on the optimized geometries.

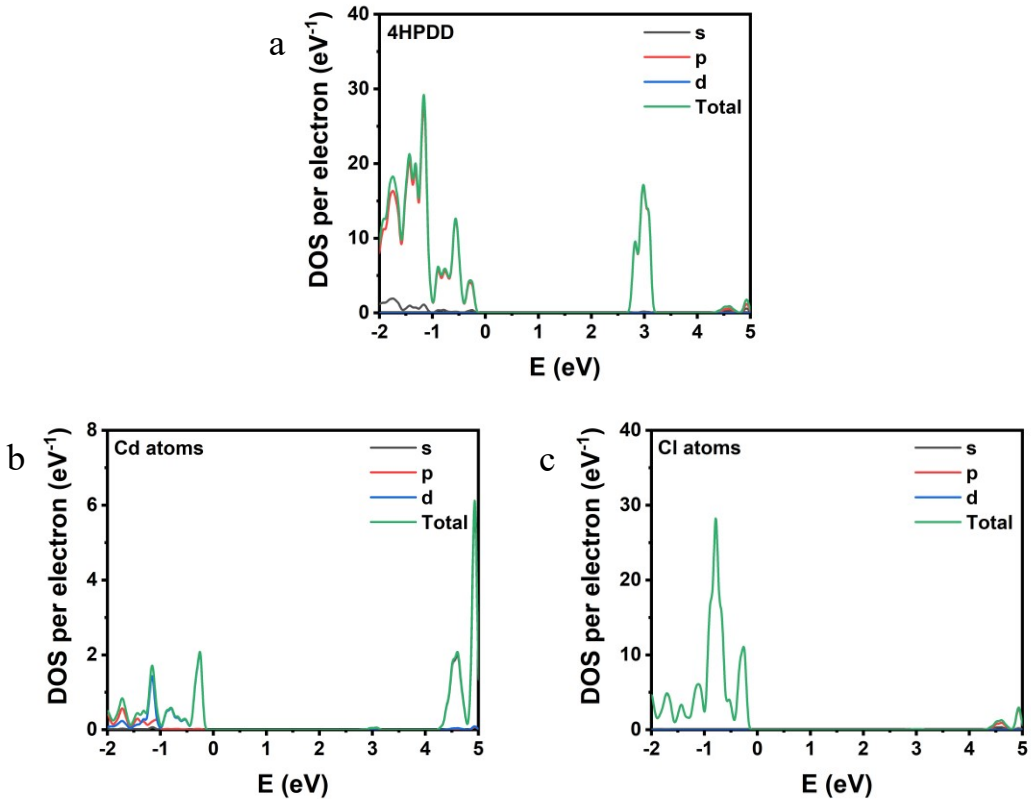

Fig. S14. (**a-c**) PDOS of the components in $CdCl_2$-4HPDD.

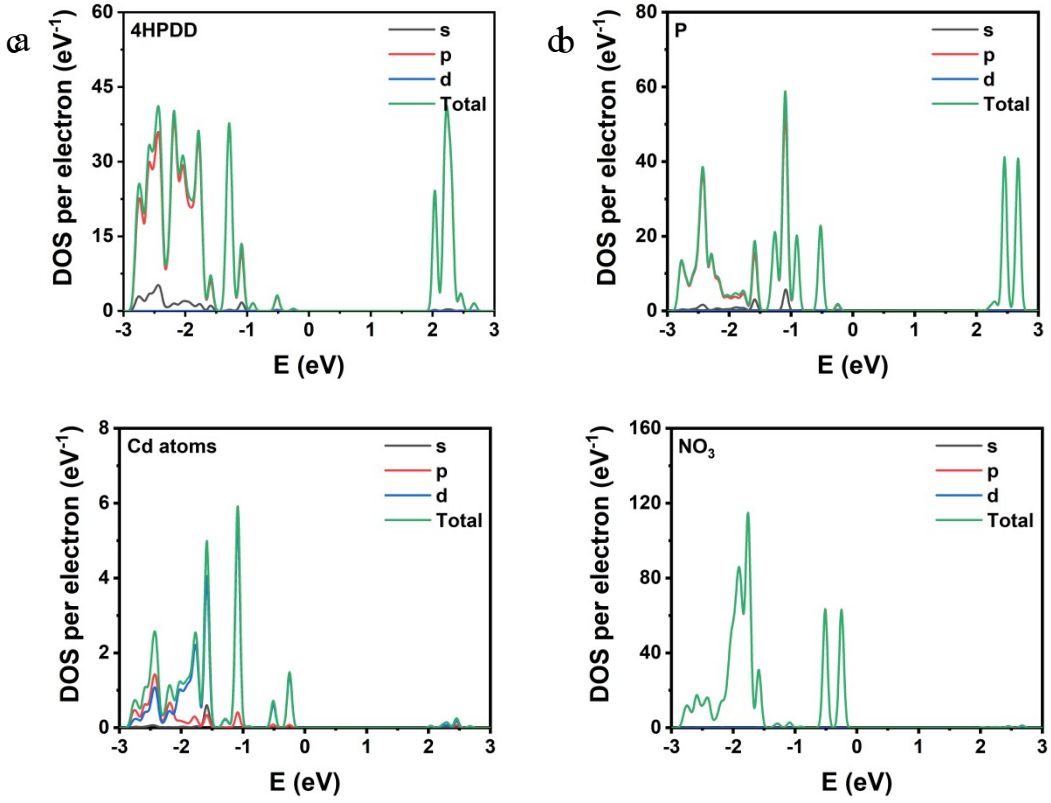

Fig. S15. (**a-d**) PDOS of the components in 4HPDD-$Cd(NO_3)_2$-P.

Total electronic density of states (TDOS) and partial electronic density of states (PDOS) reveal that the conduction bands (CB) of $CdCl_2$-4HPDD and 4HPDD-$Cd(NO_3)_2$-P both drive from the *p* orbitals of organic 4HPDD ligand while the valence bands (VB) originate from the *p* orbitals of inorganic Cl^- and NO_3^- component, respectively. This observation suggests that the nuclearity of the complexes participates in CT process, and the metal atoms (Cd) play a bridging role in chelated structure but do not contribute to VB.

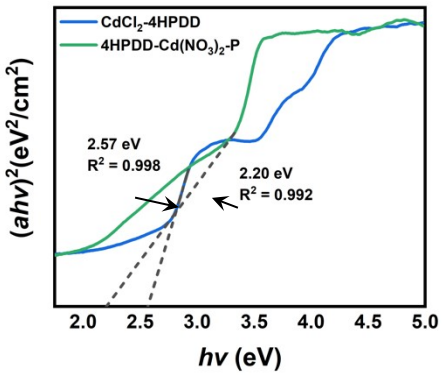

Fig. S16. The experimental band gap result based on UV-vis absorption spectra.

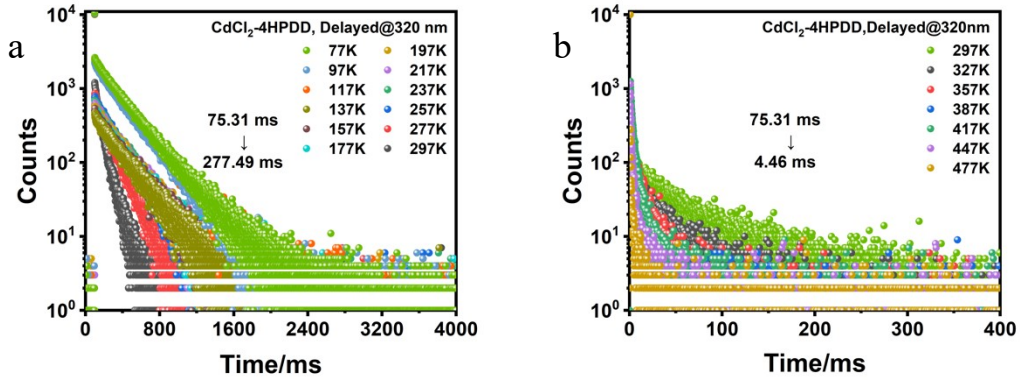

Fig. S17. The long-lived lifetime decay profiles of $CdCl_2$-4HPDD at different temperatures ranging from 77 to 297 K (a) and from 297 to 477 K (b).

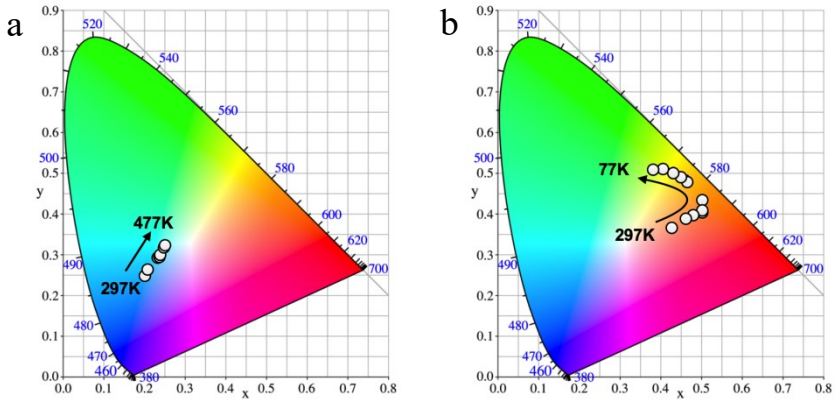

Fig. S18. Temperature-dependent luminescence of $CdCl_2$-4HPDD and 4HPDD-$Cd(NO_3)_2$-P. (a) The corresponding positions in CIE chromaticity coordinates for the prompt emission of $CdCl_2$-4HPDD. (b) The corresponding positions in CIE chromaticity coordinates for the delayed emission of 4HPDD-$Cd(NO_3)_2$-P.

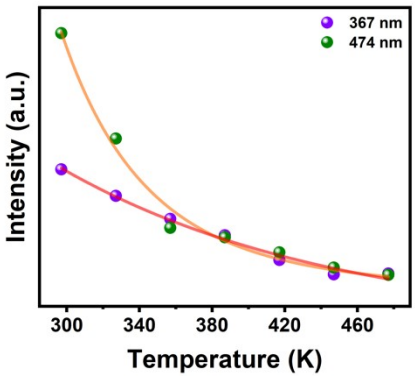

Fig. S19. Variation of the FL emission intensity of $CdCl_2$-4HPDD at 367 and 474 nm at different temperatures from 297 to 477 K.

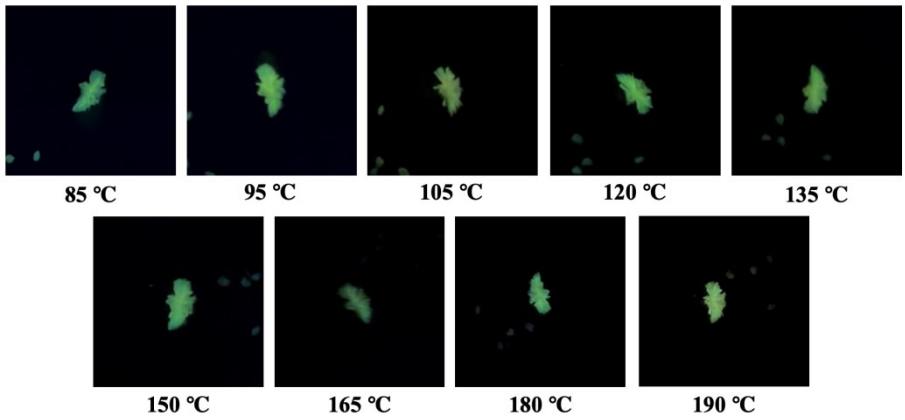

Fig. S20. The after-glow photos of $CdCl_2$-4HPDD crystals excited by 365 nm UV light at different temperatures. The luminescence can be maintained after the crystals were placed in different high temperatures (from 358 to 463 K) for 2 hours.

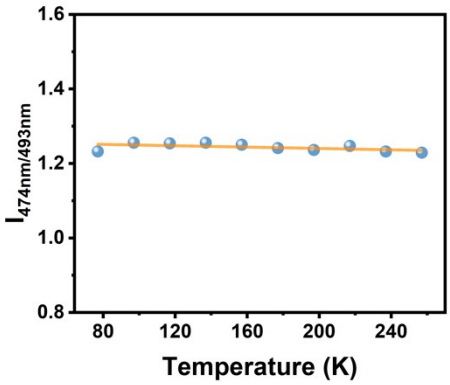

Fig. S21. Variation of the emission intensity ratio of $CdCl_2$-4HPDD between 474 and 493 nm at different temperature.

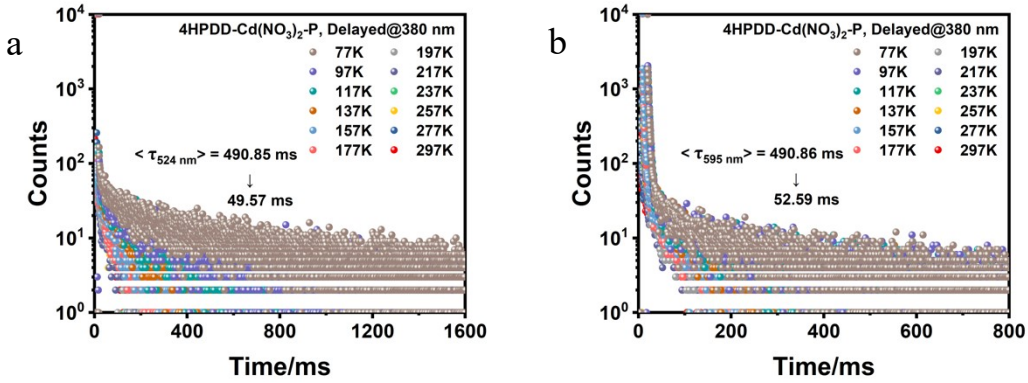

Fig. S22: The long-lived lifetime decay profiles of 4HPDD-$Cd(NO_3)_2$-P (a and b) at different temperatures ranging from 77 to 297K.

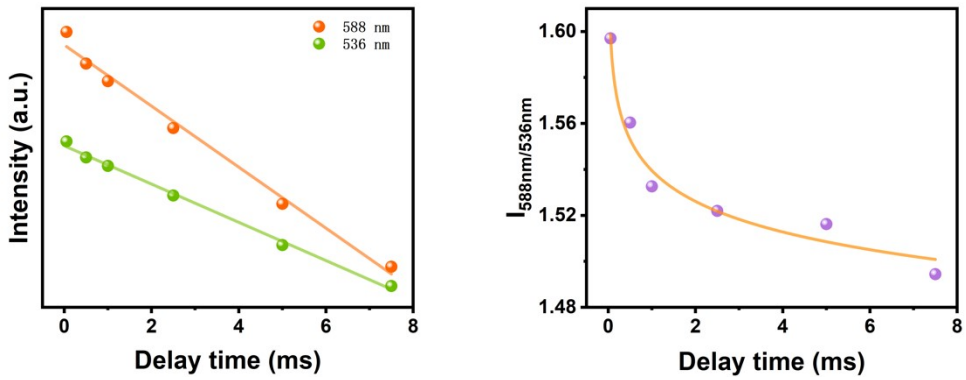

Fig. S23. Variation of the emission intensity and corresponding ratio of 4HPDD-$Cd(NO_3)_2$-P of 588 and 536 nm at different delay time at 297K.

a b

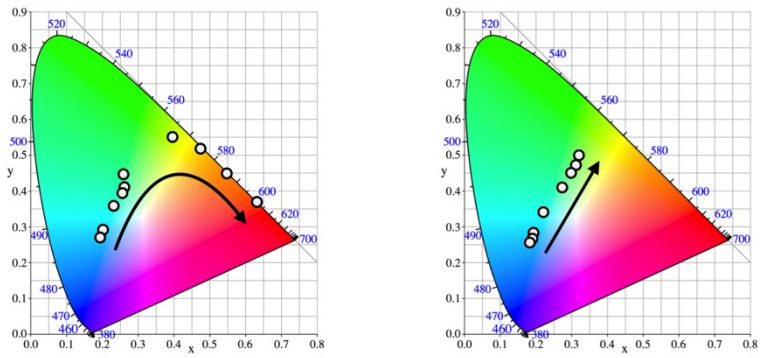

Fig. S24. The corresponding prompt (a) and delayed positions (b) of $CdCl_2$-4HPDD in CIE chromaticity coordinates.

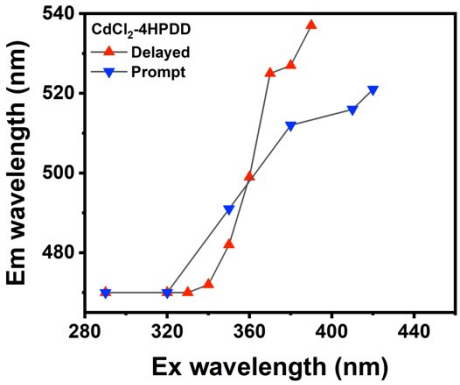

Fig. S25. The trend of prompt and delayed emission peak value when excited with changing excited light sources.

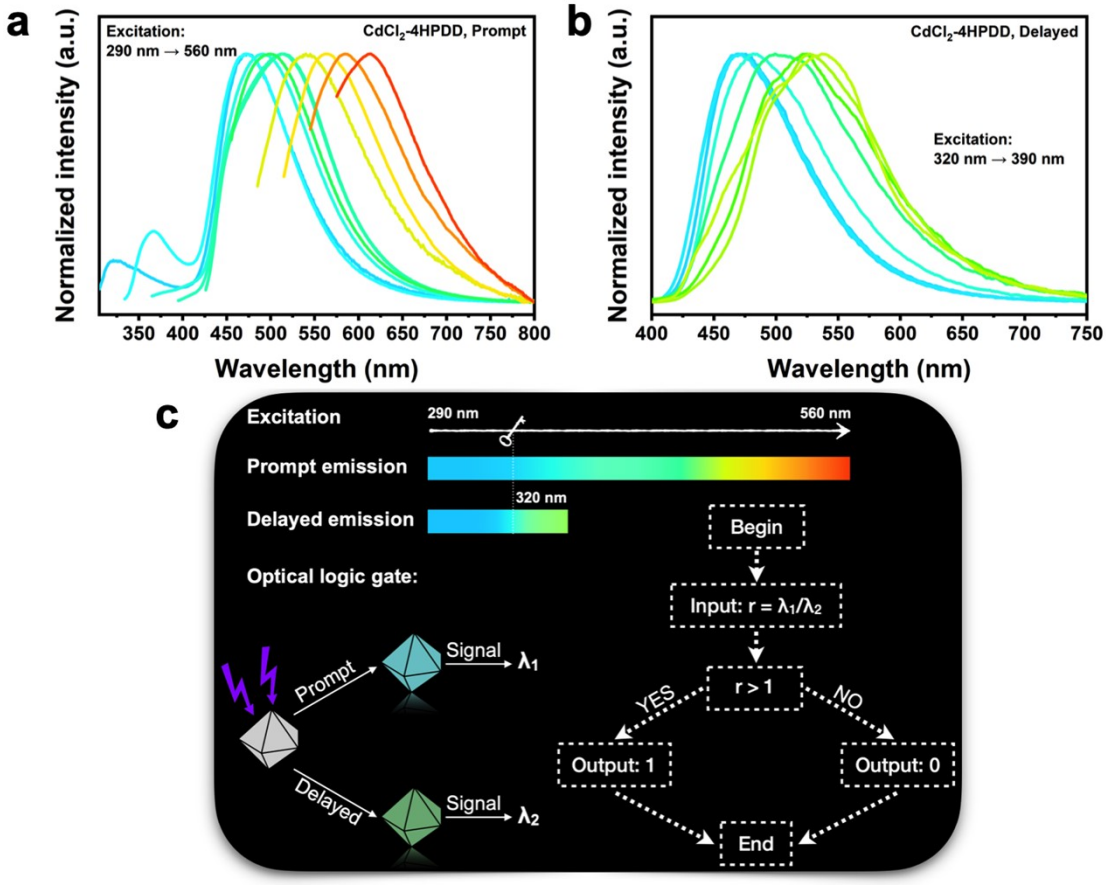

Fig. S26. Excitation-dependent prompt (a) and delayed (b) PL spectra of $CdCl_2$-4HPDD. The schematic diagram (c) for running an optical logic gate based on excited-dependent emissions of $CdCl_2$-4HPDD.

Table S1: Crystal data for $CdCl_2$-4HPDD and 4HPDD-$Cd(NO_3)_2$-P.

Sample	**$CdCl_2$-4HPDD**	**4HPDD-$Cd(NO_3)_2$-P**
Molecular Formula	$C_{18}H_{22}N_2O_{10}Cd_2Cl_4$	$C_{21}H_{17}N_5O_{11}Cd$
Molecular Weight	825.00	627.81
Temperature (K)	100.01(10)	100.01(10)
Crystal System	triclinic	monoclinic
Space Group	*P*-1	$P2_1/n$
a (Å)	8.13035(13)	11.4639(4)
b (Å)	9.45773(18)	14.5590(4)
c (Å)	10.76925(13)	14.1126(4)

α (deg)	97.5378(13)	90
β(deg)	107.1123(13)	100.388(3)
γ(deg)	114.8620(17)	90
V (Å^3)	686.37(2)	2316.83(12)
Z	1	4
GooF	1.099	1.068
D (g cm^{-3})	1.996	1.800
μ (mm^{-1})	16.549	8.220
R1 [I>2σ(I)]	0.0270	0.0543
wR2 [I>2σ(I)]	0.0723	0.1506
CCDC Number	2123501	2123507

Table S2. Selected bond distances (Å) and bond angles (º) of $CdCl_2$-4HPDD with estimated deviations (esds) in parentheses.

Bond distances (Å)			
Cd(1)-N(1)	2.3119(20)	Cd(1)-Cl(1)	2.5260(9)
Cd(1)-O(2)	2.4829(29)	Cd(1)-Cl(2)	2.6380(10)
Cd(1)-O(3)	2.5063(29)	Cd(1)-Cl(2)	2.5160(7)
Bond angles (º)			
N(1)-Cd(1)-O(2)	68.610(88)	Cl(2)-Cd(1)-O(2)	86.247(54)
N(1)-Cd(1)-O(3)	67.968(89)	Cl(1)-Cd(1)-O(2)	86.870(52)
Cl(2)-Cd(1)-O(2)	123.091(63)	Cl(2)-Cd(1)-O(3)	92.475(52)
Cl(2)-Cd(1)-O(3)	99.896(63)	Cl(1)-Cd(1)-O(3)	95.670(51)
Cl(2)-Cd(1)-N(1)	89.196(56)	Cl(2)-Cd(1)-Cl(2)	84.598(28)
Cl(1)-Cd(1)-N(1)	92.550(56)	Cl(2)-Cd(1)-Cl(1)	95.359(28)

Table S3. Selected bond distances (Å) and bond angles (º) of 4HPDD-$Cd(NO_3)_2$-P with estimated deviations (esds) in parentheses.

Bond distances (Å)			
Cd(1)-N(1)	2.3444(44)	Cd(1)-O(2)	2.5187(30)
Cd(1)-N(2)	2.3454(42)	Cd(1)-O(3)	2.5640(56)
Cd(1)-N(3)	2.3560(43)	Cd(1)-O(4)	2.3952(61)
Cd(1)-O(1)	2.5270(42)	Cd(1)-O(5)	2.4103(38)
Bond angles (º)			
N(1)-Cd(1)-O(1)	66.806(14)	O(1)-Cd(1)-N(2)	80.227(14)
N(1)-Cd(1)-O(2)	67.400(12)	O(2)-Cd(1)-N(3)	77.023(12)

N(2)-Cd(1)-N(3)	71.537(15)	O(3)-Cd(1)-O(4)	50.429(19)

Table S4. TD-DFT-calculated energy levels at singlet (S_1) and triplet (T_n) states and spin-orbit coupling (SOC) results between S_1 and T_n of $CdCl_2$-4HPDD and 4HPDD-$Cd(NO_3)_2$-P.

	$S_1 \rightarrow T_n$	S_1 (eV)	T_n (eV)	ΔE_{ST} (eV)	SOC (cm^{-1})
$CdCl_2$-4HPDD	$S_1 \rightarrow T_1$	3.7935	3.5674	0.2261	14.89
	$S_1 \rightarrow T_2$	3.7935	3.5832	0.2103	0.37
	$S_1 \rightarrow T_3$	3.7935	3.7660	0.0275	34.74
	$S_1 \rightarrow T_4$	3.7935	3.8534	-0.0599	0.23
	$S_1 \rightarrow T_5$	3.7935	3.8597	-0.0662	0.79
	$S_1 \rightarrow T_6$	3.7935	3.8941	-0.1006	15.70
	$S_1 \rightarrow T_7$	3.7935	3.9554	-0.1619	134.34
	$S_1 \rightarrow T_8$	3.7935	3.9656	-0.1721	191.03
	$S_1 \rightarrow T_9$	3.7935	4.0003	-0.2068	109.92
	$S_1 \rightarrow T_{10}$	3.7935	4.0341	-0.2406	19.49
4HPDD-$Cd(NO_3)_2$-P	$S_1 \rightarrow T_1$	3.9295	2.9274	1.0021	0.46
	$S_1 \rightarrow T_2$	3.9295	3.6017	0.3278	2.31
	$S_1 \rightarrow T_3$	3.9295	3.6346	0.2949	0.80
	$S_1 \rightarrow T_4$	3.9295	3.7437	0.1858	0.30
	$S_1 \rightarrow T_5$	3.9295	3.8044	0.1251	3.14
	$S_1 \rightarrow T_6$	3.9295	3.9313	-0.0018	1.76
	$S_1 \rightarrow T_7$	3.9295	4.0278	-0.0983	0.13
	$S_1 \rightarrow T_8$	3.9295	4.0436	-0.1141	5.43
	$S_1 \rightarrow T_9$	3.9295	4.1258	-0.1963	1.19
	$S_1 \rightarrow T_{10}$	3.9295	4.2180	-0.2885	7.74

Table S5. Photophysical parameters of $CdCl_2$-4HPDD and 4HPDD-$Cd(NO_3)_2$-P in solid-state. Fluorescence and phosphorescence spectra and lifetimes measured at 297 K. [a] k_r^{phos} represents the rate constant of radiative ($T_1 \rightarrow S_0$). [b] Singlet (E_S) and

triplet (E_T) energies estimated from the emission spectra at 297 K respectively. [c] $\Delta E_{ST} = E_S - E_T$.

	λ_F (nm)	λ_P (nm)	τ_F (ns)	τ_P (ms)	kr^{phos} (s^{-1})[a]	E_S/E_T (eV)[b]	ΔE_{ST} (eV)[c]	Φ_{PL} (%)
$CdCl_2$-4HPDD	367	474	3.57	75.31	1.14×10^3	3.39/2.63	0.76	8.58
4HPDD-$Cd(NO_3)_2$-P	420 443 470	536 588 648	3.63 3.64 4.47	49.57 52.59 49.92	1.29×10^2	2.81/2.12	0.69	0.68

3. References

1 M. J. T. Frisch, G. W.; Fox, D. J., *GAUSSAIN 09 REVISION*, 2013.

2 J.-D. Chai and M. Head-Gordon, *Phys. Chem. Chem. Phys.*, 2008, **10**, 6615-6620.

3 T. Lu and F. Chen, *J. Comput. Chem.*, 2012, **33**, 580-592.

4 Z. Liu, T. Lu and Q. Chen, *Carbon*, 2020, **165**, 461-467.

5 W. Humphrey, A. Dalke and K. Schulten, *J. Mol. Graph. Model.*, 1996, **14**, 33-38.

6 F. Neese, *Wires. Comput. Mol. Sci.*, 2012, **2**, 73-78.

7 F. Neese, *Wires. Comput. Mol. Sci.*, 2018, **8**, e1327.

8 E. vanLenthe, R. vanLeeuwen, E. J. Baerends and J. G. Snijders, *International Journal of Quantum Chemistry*, 1996, **57**, 281-293.

9 G. Kresse and J. Furthmuller, *Phys. Rev. B*, 1996, **54**, 11169-11186.

10 J. P. Perdew, K. Burke and M. Ernzerhof, *Phys. Rev. Lett.*, 1997, **78**, 1396-1396.

11 D. J. Chadi, *Phys. Rev. B*, 1977, **16**, 1746-1747.

12 S. Grimme, J. Antony, S. Ehrlich and H. Krieg, *J. Chem. Phys.*, 2010, **132**, 154104.